Mesoscale Simulations of Surfactant Dissolution and Mesophase Formation

P. Prinsen,[1,2] P. B. Warren,[1] and M. A. J. Michels[2]

[1]*Unilever Research and Development Port Sunlight, Bebington, Wirral CH63 3JW, United Kingdom*

[2]*Department of Applied Physics, Eindhoven University of Technology, P.O. Box 513, 5600 MB Eindhoven, The Netherlands*

(Received 24 April 2002; published 11 September 2002)

The evolution of the contact zone between pure surfactant and solvent has been studied by mesoscale simulation. It is found that mesophase formation becomes diffusion controlled and follows the equilibrium phase diagram adiabatically almost as soon as individual mesophases can be identified, corresponding to times in real systems of order 10 μs.

DOI: 10.1103/PhysRevLett.89.148302 PACS numbers: 82.70.Uv, 05.90.+m, 61.30.St, 64.70.Md

When pure surfactant comes into contact with water, mesophases appear at the interface. This is an important process not only for the practical use of surfactants, but also from the point of view of fundamental surfactant phase science. Indeed, contact "flooding" or penetration scan experiments can yield quantitative information on mesophases as a function of composition [1]. The phenomenon seems to be invariably *diffusion controlled* in the sense that the widths of the mesophases follow $t^{1/2}$ growth laws, and *adiabatic* in the sense that the local composition determines the mesophase boundaries according to the equilibrium phase diagram [2–4]. But penetration scan experiments are restricted to observation times of minutes to hours: What happens on time scales shorter than this? How early does diffusion control set in, and how soon can one expect the mesophase boundaries to track the local composition adiabatically? Such questions are not just of scientific interest since time scales of seconds or less are important in modern processing and the everyday use of surfactants, for instance, determining how rapidly washing powder dissolves. Experimentally, this regime is very difficult to access because of the short time scales and the relatively small amounts of mesophase involved. To probe these questions, we have therefore undertaken novel mesoscale simulations of surfactant dissolution. We find adiabatic diffusion control is established remarkably rapidly in our model, on time scales in which only a few repeat units of the growing mesophases have appeared, corresponding to times in the real systems of order 10 μs.

The model we have used is a "minimalist" particle-based model of a binary surfactant/water mixture [5], based on the dissipative particle dynamics (DPD) method [6,7]. In DPD, the particles are soft spheres, interacting with pairwise soft potentials of the form $U = \frac{1}{2}A(1 - r/r_c)^2$ $(r < r_c)$, where r is the particle separation, r_c is the range of the interaction, and A the amplitude. In the model, we have three species of particles: A, B, and C. The A and B particles are bound together in pairs as dimers with a fixed separation r_d, and represent the surfactants. The C particles are monomers representing the solvent (water). The different species are distinguished by their interaction amplitudes, and the trick is to find a set of amplitudes which recover suitable phase behavior. Following earlier work [7], we use $A_{AA} = A_{BB} = A_{CC} = 25$, $A_{AB} = 30$, $A_{AC} = 0$, $A_{BC} = 50$, and $r_d = 0.5$ which gives phase diagram features lying in a convenient temperature range around $k_BT \sim 1$ (we fix units by choosing $m = r_c = 1$, where m is the mass of the particles).

Figure 1 shows the phase diagram as a function of dimer concentration and k_BT, at an overall density $\rho = (2N_{AB} + N_C)/V = 6$, where dimer concentration is defined to be the mole fraction of particles in dimers, $c = 2N_{AB}/(2N_{AB} + N_C)$. Similar to many real systems [8], micellar (L_1), hexagonal (H_1) and lamellar (L_α) phases are found in order of increasing dimer concentration. We have also tuned the interactions so that on the pure dimer side there is a reentrant isotropic fluid (L_2) phase, since this reflects the real behavior of many nonionic surfactants and is crucial to the contact simulations below. We did not find any cubic phases, although we note that these are not always present in real systems [8,9] (an extensive study of lattice models by Larson [10] suggests that cubic phases could be engineered to appear, particularly if the present model is elaborated beyond dimers). Also, we caution that k_BT in the model is not easily mapped onto a real temperature. Despite these deficiencies, it is nevertheless remarkable that such a simple model reproduces the main features of the phase diagram common to a large number of surfactants.

To simulate surfactant dissolution and mesophase formation is now very simple. We take two simulation boxes, one containing an equilibrated fluid of pure dimers and the other containing equilibrated solvent particles. We place them next to each other and allow the dimers and solvent particles to interdiffuse. Just as in the real systems, mesophases start to appear at the interface over time. Here we report results for the $k_BT = 1$ isotherm; the $k_BT = 0.5$ isotherm was also studied with similar results. We consider simulation boxes of size $10^2 \times 100$, with the concentration gradient along the long axis. Figure 1 shows some representative simulation snapshots.

While this is straightforward, there are a couple of technical points to be considered. First, it is important

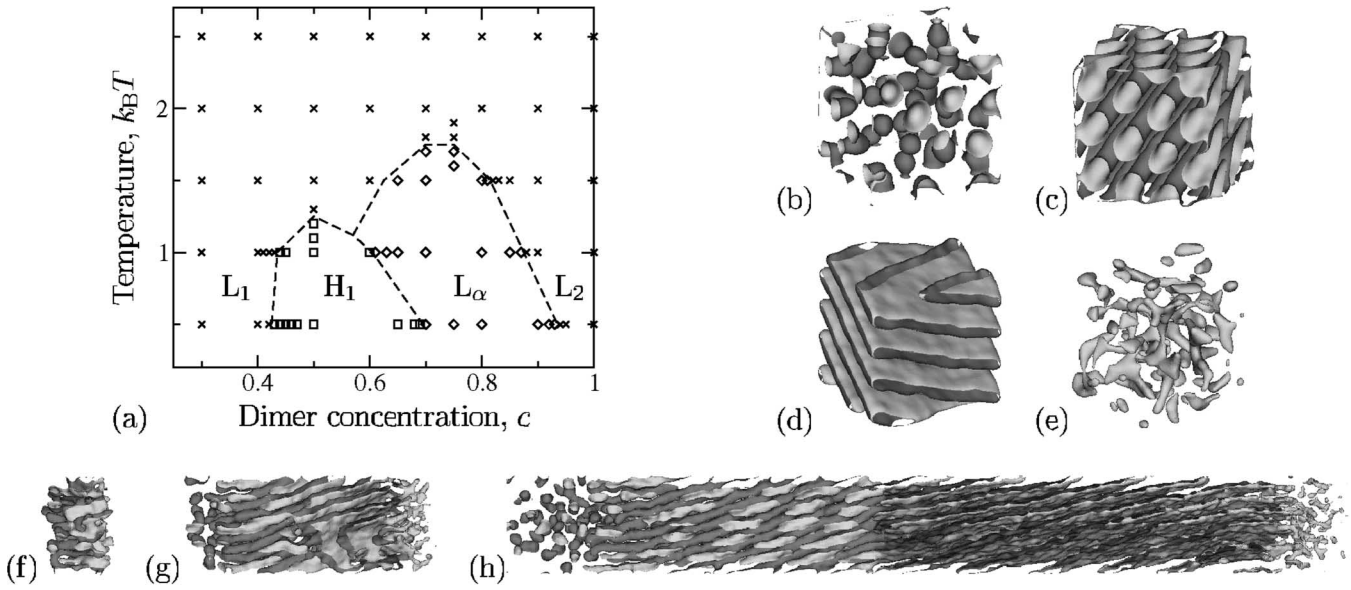

FIG. 1. (a) Phase diagram for dimer/solvent model in (c, k_BT) plane showing points where we find isotropic, hexagonal, and lamellar phases (crosses, squares, and diamonds, respectively). The lines are a guide to the eye. (b)–(e) Isosurfaces ($\rho_C = 1.3$) for equilibrium phases along $k_BT = 1$ isotherm, at $c = 0.3$, 0.6, 0.7, and 0.9, respectively. (f)–(h) Isosurfaces showing snapshots of surfactant dissolution simulations, at elapsed times $t = 12$, 120, and 1200 DPD time units from initial contact.

to adjust the densities in the two boxes so that the pressures are equal. From separate simulations, we determined the equation of state for the pure components, and found that densities $\rho = 6.124$ and 5.896 for the solvent and dimers, respectively, give a common pressure $p \approx 100$. These densities are within $\approx 2\%$ of the density $\rho = 6$ used to construct the phase diagram of Fig. 1, which obviates the need to consider constant pressure simulations. The pressure matching is important though because it suppresses sound waves which would spoil the subsequent analysis. Second, if we were to use conventional periodic boundary conditions, there would be an unwanted second interface in the system. We eliminate this by bounding the simulation box in the long direction by hard reflecting walls, supplemented by short-range soft repulsive potentials of the form $U = \frac{1}{2}A_{\text{wall}}(1 - z/r_c)^2$ $(z < r_c)$, where z is the distance from the hard wall. The soft repulsive force suppresses density oscillations which would otherwise arise due to the abrupt termination of the particle density. We find empirically $A_{\text{wall}} = 25$ gives a smoothly vanishing density. Periodic boundary conditions are retained in the other two directions.

Now we turn to an objective analysis of the simulations to determine the growth laws. This is done by introducing a local order parameter which can distinguish between mesophases as a function of distance normal to the original contact plane. We examined various possibilities, such as the use of topological (Minkowski) functionals [11,12], but an approach which works well in practice is motivated by the $\rho_C = 1.3$ isosurfaces shown in Fig. 1. The different mesophases are clearly distinguishable to the eye because the isosurface is predominantly spherical, cylindrical, planar, or fragmented, for the L_1, H_1, L_α, and L_2 phases, respectively [13]. This geometric insight can be made quantitative by constructing the second moment of the isosurface normal distribution $p(\mathbf{n})$, namely, the symmetric tensor $\mathbf{M} = \int \mathbf{nn}\, p(\mathbf{n}) d\mathbf{n}$ [14]. The local geometric nature of the isosurface and, hence, the underlying mesophase is reflected in the eigenvalues μ_i of $\mathbf{M}$ [15]. If these eigenvalues are ranked in order of increasing size, we determined after some trials that a slice can be classified as H_1 if $\mu_1 < 0.05$ and $\mu_{2,3} > 0.3$, or L_α if $\mu_1 < 0.05$ and $\mu_2 < 0.15$ (note $\sum_{i=1}^{3} \mu_i = 1$).

For the present study, we divide the simulation box into slices of thickness $0.25r_c$ parallel to the original contact plane and determine the eigenvalues of $\mathbf{M}$ for each slice. Figure 2(a) gives a representative example, showing that the various mesophases can be clearly distinguished. The transition between H_1 and L_α is particularly sharp as can also be seen in Fig. 1(h) [16]. The above criteria are used to classify each slice and the positions of the boundaries between mesophases determined as a function of time. There is a short incubation period before the local order parameter can distinguish the different mesophases, but, beyond this point, the boundaries can be reliably tracked as shown in Fig. 2(b). The key results are contained in Figs. 2(c) and 2(d), which show, respectively, the local composition at the mesophase boundary and the squared width of the middle two mesophases as a function of time.

Figure 2(c) shows that the local compositions become established at constant values almost as soon as mesophases can be distinguished. These values are

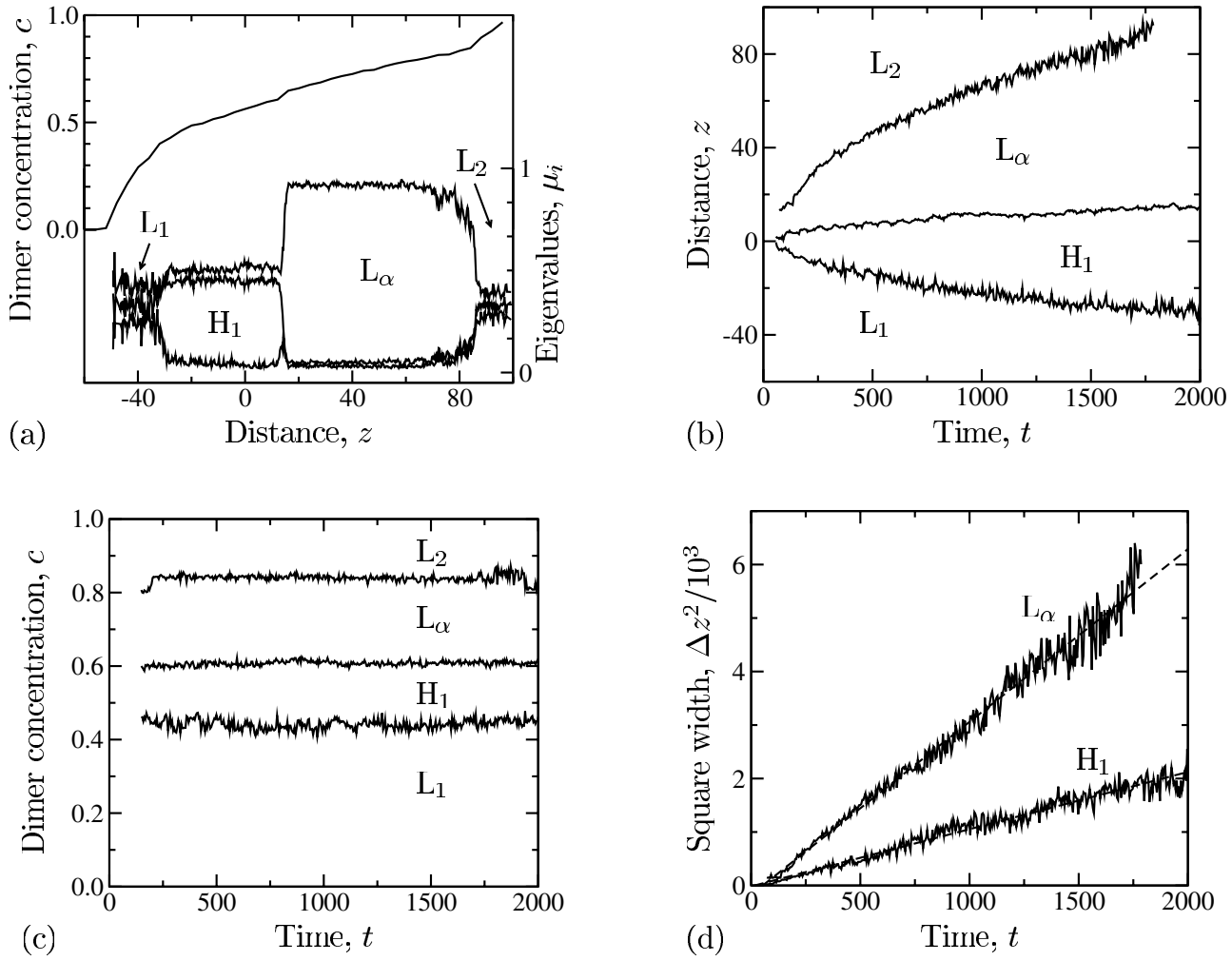

FIG. 2. (a) Concentration profile (upper curve) and eigenvalues of local order parameter tensor (lower curves) at $t = 1200$ DPD time units after initial contact. (b) Phase boundary positions as a function of time, as determined from the eigenvalue analysis. (c) Local concentrations at phase boundaries, and (d) squared widths of middle mesophases, as functions of time.

$c = 0.44(1)$, 0.61(1), and 0.84(1), for the L_1-H_1, H_1-L_α, and L_α-L_2 boundaries, respectively, (the number in brackets is an estimate of the error in the final digit). These should be compared to the equilibrium transition concentrations $c = 0.435(5)$, 0.605(5), and 0.875(5) read off Fig. 1(a). Thus, the L_1-H_1 and H_1-L_α boundaries in the kinetic simulation lie almost exactly at the point expected from the equilibrium phase diagram. The L_α-L_2 boundary is displaced from that found in the equilibrium phase diagram, but it is clear from Fig. 2(a) that this boundary is not completely sharp. Apart from this boundary therefore, it appears that the mesophases grow adiabatically almost from the earliest moments that the local order parameter can distinguish the growing mesophases.

Figure 2(d) shows that both mesophases follow a $\Delta z^2 = \beta(t - t_0)$ law, where Δz is the mesophase width. This is a classic test and suggests that the process of mesophase growth is diffusion controlled from the earliest times for which mesophases can be distinguished. The straight line fits in Fig. 2(d) have slopes $\beta = 1.07(1)$ and 3.23(2) for the H_1 and L_α phases, respectively ($t_0 \lesssim 50$ for both). To further examine this, we fit β to what would be expected if the local composition followed a simple diffusion law $c = (1 + \mathrm{erf}(z/\sqrt{4D_{\mathrm{eff}}t}))/2$, where D_{eff} is an *effective* diffusion coefficient. This would predict $\beta = 4D_{\mathrm{eff}}[\mathrm{erf}^{-1}(2c_2 - 1) - \mathrm{erf}^{-1}(2c_1 - 1)]^2$, where $c_{1,2}$ are the fixed compositions at the edges of the mesophase of interest. We find $D_{\mathrm{eff}} = 3.0(5)$ and 3.2(4) for the H_1 and L_α phases, respectively. These effective diffusion coefficients are, within statistical errors, the *same* in the two phases. This is similar to previous experimental findings [3]. Note though that the concentration profiles, such as those shown in Fig. 2(a), do not fit the simple diffusion law suggesting that D_{eff} is not constant across all compositions and all phases.

For comparison, we also determined from separate simulations the self-diffusion coefficients for the two pure components. We find $D_{\mathrm{self}} = 0.219(3)$ for solvent particles in pure solvent, and $D_{\mathrm{self}} = 0.092(2)$ for dimers in a pure dimer fluid. The effective diffusion coefficients

in the mesophases are considerably greater than these which suggests the existence of a sizable free energy driving force enhancing diffusion and is reminiscent of a detailed study on the H_1 phase of the $C_{12}E_6$/water system [17].

We can use D_{eff} to map elapsed times in our mesoscale simulation onto real times. For example, for nonionic surfactants, it was found experimentally $D_{\text{eff}} \approx 2 \times 10^{-10}\ \text{m}^2\,\text{s}^{-2}$ [3]. The lamellar repeat spacing L can be used as a common measure of length: $L \approx 2.5$ DPD units in the simulation, and $L \approx 5$ nm is typical for real systems. By using L^2/D_{eff} to scale time, we conclude one DPD time step is approximately equivalent to 50 ns. Thus, the duration of the whole simulation (2000 DPD time units) represents more than 0.1 ms of real time, equivalent to 10^{11} molecular dynamics time steps. Our results suggest that adiabatic diffusion controlled dissolution sets in after about 200 DPD time units, equivalent to about 10 μs, which is the origin of the time scale quoted in the introduction.

Our simulations, while addressing very directly intriguing questions concerning surfactant dissolution, are also interesting because they are simulations of phase formation kinetics starting from a highly inhomogeneous state [18,19], rather than the usual approach which is to quench a homogeneous system [20]. It is indeed striking that we do *not* find any evidence of metastability which would delay the appearance of the mesophases (in contrast to what is sometimes found in temperature-jump experiments [21]), nor do we find any systematic displacement of the mesophase boundaries by the strong concentration gradients present at such early times. Furthermore, previous studies of front propagation in unstable media might suggest that our mesophase boundaries should propagate with some asymptotic constant velocity [22,23], but all the evidence in Fig. 2 suggests propagation is limited by the interdiffusion of the two species in our model and not by phase formation kinetics. For example, the motion of the L_α-L_2 boundary in Fig. 2(b) could be fitted to a constant-velocity growth law at late times, but we do not find this convincing since an equally good fit can be made to a diffusive growth law over the *whole* time period.

Finally, our mesoscale model is also well suited to other large-scale phenomenological studies of surfactant (meso)phases, such as temperature quenches, the effect of shear, more detailed exploration of epitaxial relationships, among many other possibilities.

[1] R. G. Laughlin, Adv. Colloid Interface Sci. **41**, 57 (1992).

[2] P. B. Warren and M. Buchanan, Curr. Opin. Colloid Interface Sci. **6**, 287 (2001).

[3] B. H. Chen, C. A. Miller, J. M. Walsh, P. B. Warren, J. N. Ruddock, P. R. Garrett, F. Argoul, and C. Leger, Langmuir **16**, 5276 (2000).

[4] R. G. Laughlin and R. L. Munyon, J. Phys. Chem. **91**, 3299 (1987).

[5] J. C. Shelley and M. Y. Shelley, Curr. Opin. Colloid Interface Sci. **5**, 101 (2000).

[6] R. D. Groot and P. B. Warren, J. Chem. Phys. **107**, 4423 (1997).

[7] S. Jury, P. Bladon, M. Cates, S. Krishna, M. Hagen, J. N. Ruddock, and P. B. Warren, Phys. Chem. Chem. Phys. **1**, 2051 (1999).

[8] R. G. Laughlin, *The Aqueous Phase Behavior of Surfactants* (Academic, New York, 1994).

[9] D. J. Mitchell, G. J. T. Tiddy, L. Waring, T. A. Bostock, and M. P. McDonald, J. Chem. Soc. Faraday Trans. **79**, 975 (1983).

[10] R. G. Larson, J. Phys. II (France) **6**, 1441 (1996).

[11] K. Michielsen and H. de Raedt, Phys. Rep. **347**, 461 (2001).

[12] A. Aksimentiev, M. Fiałkowski, and R. Hołyst, Adv. Chem. Phys. **121**, 141 (2002).

[13] Since we use the solvent isosurface $\rho_C = 1.3$, we are looking at fragmented solvent domains in the dimer-rich L_2 phase in Fig. 1(e) and the right-hand sides of Figs. 1(f)–1(h). The absence of long range order in the L_2 phase has been checked elsewhere [7].

[14] This is easy to implement since isosurface normals are used in the lighting model to generate the images, and a representative sample can be extracted by intercepting the graphics pipeline: W. Schroeder, K. Martin, and B. Lorenson, *The Visualisation Toolkit* (Prentice Hall, New Jersey, 1998). A similar order parameter could be constructed from the dimer orientation distribution function.

[15] K. V. Mardia, *Statistics of Directional Data* (Academic, New York, 1972).

[16] Closer examination of the H_1-L_α boundary indicates an epitaxial relationship in which the lamellae break up into a hexagonal array of rods oriented approximately normal to the boundary, similar to the tines on a comb. Note also there is a small jump in the concentration profile across this boundary, shown, for example, in Fig. 2(a), which could be interpreted as the signature of a very weak first order phase transition unresolved by our equilibrium studies.

[17] L. Sallen, P. Oswald, and P. Sotta, J. Phys. II (France) **7**, 107 (1997).

[18] W.-J. Ma, P. Keblinski, A. Maritan, J. Koplik, and J. R. Banavar, Phys. Rev. Lett. **71**, 3465 (1993).

[19] W. R. Osborn, E. Orlandini, M. R. Swift, J. M. Yeomans, and J. R. Banavar, Phys. Rev. Lett. **75**, 4031 (1995).

[20] A. J. Bray, Adv. Phys. **43**, 357 (1994).

[21] M. Clerc, P. Laggner, A.-M. Levelut, and G. Rapp, J. Phys. II (France) **5**, 901 (1995).

[22] G. Dee and J. S. Langer, Phys. Rev. Lett. **50**, 383 (1983).

[23] W. van Saarloos, Phys. Rev. A **37**, 211 (1988).